

NIH Public Access

Author Manuscript

Magn Reson Med. Author manuscript; available in PMC 2016 February 01.

Published in final edited form and

M. sn Reson Led. 2015 February ; 7. (2): 622-632. doi:10.1002/mrm.25175.

Optimized Three Dimensional Sodium Imaging of the Human Heart on a Clinical 3T scancer

Neville J. Gein, Carlos Pophitte², Marcelo J. Nacif³, and David A. Bluemke^{1,4}

¹Radiology & Imaging Sciences, National Institutes of Health, Eethesda, MD, USA

²Heart Institute, InCor, University of São Paulo Medical School and HCOR - Hospital do Coração, São Paulo Brazil

³Federal Humir ense University, School of Medicine, Pic de Janeiro, Brazil

⁴NIBIB, Bethesda, MD, UGA

Abstract

Purpose—Optimization of sequence and sequence parameters to allow 3D sodium imaging of the entire hum in heart in-vivo in a clinically reasonable time

Theory and Mathe ds—A stack of spirals pulse sequence was optimized for cardiac imaging by considering factors such as spoiling mutation angles, repetition time cono time, T1/T2 relaxation, off-resonance, data acquisition window, motion and segmented k-space acquisition. Simulations based on Bloch equation: as well as the chart trajectory used for data acquisition provided the basis for choice of parameter combination; for sodium imaging. Schum phontom scanning was used to validate the choice of parameters and for corroboration with circulations. In-vivo cardiac imaging in six volunteers was also done with an optimized sequence.

Results—Phantom studies showed good correlation with simulation cosults. Images obtained from human volunteers showed that the heart can be imaged with a nominal resolution of $5 \times 5 \times 10 \text{ mm}^3$ and with SNR>15 (in the septum) in about 6-10 minutes. Long axis views of the reformatted human heart show the 3D imaging capability.

Conclusion—Optimization of the sequence and its parameters allowed in-vivo 3^D sodium imaging of the entire human heart in a clitically reasonable time.

Keywords

sodium MRI; heart; 3D imaging

Introduction

Tissue viability after an ischemic even is an important det irminant in the discision to intervene with corrective measures (such as angion¹ asty circoronary bypass graft) in an effort to reperfuse the affected myopardianussue (1). Sodium imaging provides a direct

Corresponding Author Neville Gai, Ph.D., Radiology and Imaging Science⁶ (AD \perp IS), ⁶ J00 Rockville Pike, Bldg 10, National Institutes of Health/Clinical Center, Bethesda, MD 20892, Phone: (3(1) +J2-5114 / Fax: (J01) 496-0°, 3, gaind@cc.nih.gov.

Gai et al.

window into cell visibility drougn attered functioning of the sodium pump. Under normal circuitistances, the sodium pump maintains a gradient across the cell membrane whereby the catrace lular concentration (-140 mm -01/1) is much greater than intracellular concentration (-140 mm -01/1) is much greater than intracellular concentration (-140 mm -01/1) is much greater than intracellular concentration (-140 mm -01/1) is much greater than intracellular concentration (-140 mm -01/1) is much greater than intracellular concentration (-140 mm -01/1) is much greater than intracellular concentration (-140 mm -01/1) is much greater than intracellular concentration (-140 mm -01/1) is much greater than intracellular concentration (-140 mm -01/1) is much greater than intracellular concentration (-140 mm -01/1) is much greater than intracellular concentration (-140 mm -01/1) is much greater than intracellular concentration (-140 mm -01/1) is much greater than intracellular concentration (-140 mm -01/1) is much greater than intracellular concentration in the set of sodium lises considerably (by almost threefold) resulting in -100 mm -01/1 and -100 mm -01/1 is a gradient signal with line lunger than a readimension of sodium line -100 mm -01/1 is a gradient signal with line -100 mm -01/1 in the area is completely occluded. Since sodium imaging provides a direct window into cell membrane viability, it can be an early and sensitive indicator in caller, stroke and invocential infarction (3,4).

Societte nacteus has the second highest (second only to hydrogen) NMR sensitivity invive ²³Na has a lower gyromegatetic ratio (=25% or ¹H) and lower in-vivo concentration. For example, concentration of sodium in healthy myoca dial tissue is 43 mmol/l (1 liter of water = 111 moleco of H⁺) (5). The signar from in-vivo societum in myocardium is then about 12000 times lower than proton signal. Consequently, ³Na imaging suffers from poor signalto-noise ratio and increased scan times. A result of the lower gyromagnetic ratio is that B1 field required to induce nutation needs to be consequently higher (since $\alpha = \gamma \int B1(t)dt$). The softium coil therefore typically has a higher P1 limit than the proton coil (B1 limit twice as high for ²³Ne as 'H for our coil). The excitation put is stretched by a factor of two to achieve the same nutation for sodium essuring operation at peak B1 to keep pulse duration at runnin run. SAR increases proportionately as the square of the peak RF utilized. Therefore, SAK deposition in sodium imaging is approximately four times that in proton imaging.

Most techniques used to date rely on non-Cartesian trajectories to reduce echo time. For example, ramal imaging has been used for studying the brain (4), heart (7), kidneys (8) and skeletal muscle (9). Boada et al. (10) have previously used a twisted projection technique for brain imaging while Organ erkerk et al. (11) have presented a similar technique for cardiac sodium imaging. Few studies of 3D imaging of the neart have been come to-date. Pabet et al. (12) used a spotted gradient echo sequence to obtain 5D images of the heart in about 58 minutes. Similarly, sandstede et al. (13) studied the time course of 23Na signal intensity after myocardia minarction using an EC/2 triggered 3D gradient echo sequence with a scan time of 30 min for six slices of 3D radial projection technique was used by Jerecic et al (14) for cardiac imaging. Very recently, a stack of spirals has been used to perform sodium brain imaging at 7T (15).

To our knowledge, few studies have been done to optimize bequence and acquisition parameters especially for coulum *cordiac* magnetic resonance imaging. Lact the pardiac triggering leads to shorte. Acquisition time but tringging is typically employed (5,16) to reduce cardiac motion and blurring due to averaging of the systolic and diastellic plases of the heart (17). The need to perform triggering entails imaging in the non-steady state although constant rf excitation schemes car overcome this limitation. In this study, we first carried out a systematic optimization (for SNP_time) of plase sequence praemeters including flip angle, echo train length (*ed*), echo time, repetition time, desired resolution and data acquisition window. Simulat ons were carried out to reasure the point splech function (PSF) for a given acquisition based on the exact 1: space trajectory of the spiral dequence Simulation results were corroborated with results from imaging; studies using a single channel sodium coil at 3T.

Theory

Case for Spire' Incging

Spit 1 in aging (18-21) provides time efficient k-space coverage and has several advantages especially for sodium imaging. Chief among them are the possibility of reduced echo time (since the trajectory bigs a $\mathbf{k} = 0$) and reduced motion artifacts. In addition, the absence of off-r sonar' species such as signal from fat and the much reduced B₀ field inhomogeneity artifact (by virtue of gyr agnetic ratio being approximately 1/4 of ¹H) provide an ideal cranbination of circumstances for sor jum imaging. Reduced off-resonance artifact allows for longer data a quisition willows. Motion artifacts are also much reduced as in proton imaging due to the inherent infocusing of gradient morients in spiral imaging. In addition, reduced gyromagnetic ratio (when compared with proton imaging) will lead to reduced dephasing or spins and therefore reduced artifacts. Priviously described sodium imaging studie in the cart have used the 2D (7) or 3D r dial (14) acquisition technique. While a tru 3L re and te annique (such as a cushball geometry) does enjoy the advantages of a very shot echo time, it is not as efficient for k-space coverage. The volume scanned is spherical 2.1d prote to aliasing artifacts unless a large number of spokes are acquired. The geometry covered by 2D stack of spirals imaging is cylindric which is conducive to complete cardiac coverage, especially when employing anisotropic resolution along the long axis. A longer scavning window has other advantages in that the percentage of time spent acquiring data per repetition time increases since duration of KF and emisne, gradients stay roughly constant.

The k-space trajectory for spiral is defined by (22,23)

 $k(t) = A\lambda(t) \exp(j\lambda(t) + j_{\lambda}\lambda_{0})$

 λ_0 is the spiral angle at the origin; $\lambda_0 = 2\pi/N_s$, where N_s is the manber of spiral arms. $\lambda(t)$ is the pitch of the spiral. A = $k_{max}/(2\pi N_\tau)$ where N_τ is the number of revolutions required to reach maximum pitch of $\lambda_{(1)max} > 2\pi N_c$ and $j = \sqrt{-1}$. The initial part of the spiral has constant angular velocity will be the latter part is traversed with constant linear velocity. The function $\lambda(t) = \Omega t (1+t/T)^{-1/2} d$ scribes such, spiral where it determines the transition from constant angular velocity (when $t \ll T$) to constant linear velocity (where $t \gg T$). T is found by optimization such that the velocity and acceleration in k-space remain just with the limits set by the gradient system.

Gradient Echo Variants

Two popular variations of gradient-echo imaging for the spiral trajectory are considered. The first (labeled as sequence A) is a gradient echo sequence where a large constant dephasing gradient (24) is applied after the acquisition and the phase encoding gradient i. rephased after the echo (also known as SSFP rID of rISP) while the second is the standard sported gradient echo similar to (A) except the RF spoiling is employed. The latter sequence is labeled sequence B in this work.

In the first case, a large but constant gradient is arrived at the end of each TR while the NF pulses have the same phase. The large constant gradient provides a certain distribution of the

Gai et al.

phase φ of the transmission magnetization within a voxel. As shown by Buxton (25), if the gradient area is large enough, it is casonable to assume that φ is distributed uniformly over the voxel. The resulting signal can than be calculated using the formulation from (26,27):

$$M\left(n+1\right) = \frac{1}{2\pi} \left[\int R_{z}\left(\varphi\right) c\left(\iota, T1, r^{2}\right) R_{x}\left(\alpha\right) d\varphi \right] M\left(n\right) + \left(1 - E_{1}\right) M_{0} \quad [2]$$

 $R_{\perp}(\varphi)$ refus to the phase dispersion $R_{x}(\tau)$ is the rotation resulting from the RF pulse α , while S(t, T1, T2) corresponds to relevant m_{\perp} (see Appendix for detailed definitions); M(n+1)and M(n) are the magnetization values before and at the end of a given TR. $E_{I} = \exp(-t/T1)$ and M_{0} is the equilibrium n agnetization. An optimized train of excitation angles is difficult to derive in this case. Unless 1 R >> T2, ooth longleudical and transverse spins will contribute to the magnetization in the period TR

The more raminar should sequence (labeled as dequence B) employs a RF spoiling scheme such that the transverse magnetization at the end of each sequence is essentially zero. The magnetization evolution is given by

$$M_{z}(n+1) = M_{z} n E_{1} \cos \alpha - (1-E_{1})M_{0}$$

$$M_{v}(n+1) = M_{z}(n)E_{2} \sin \alpha$$
[3]

Flip angle

A constant fup angle train employed with the spoiled gradient - cho spiral scheme (sequence B) will let d to a filtering effect the transverse magnetization values from one TR to the next. To reduce this valuation, an iterative scheme can be comployed to derive the flip angle train (28) whereby

$$\alpha_{n+1} = \sin^{-1} \left[\frac{\sin \alpha_0 \tan \alpha_n}{F_1 \sin \alpha_0} - \left(1 - F_1 \right) \tan \alpha_n \right]$$
 [4]

As noted, with sequence A, there is no standard solution to r constant riagnetization. Consequently, a filtering effect can occur (basid on T1 value) regulting in olurring.

Relaxation Effects

Sodium exhibits biexportantial T2 relaxation vither short component (~0.5-5 cm) and a longer component (~20 n c) at 3T (29,30). Typically 60% of the signal contrabution comes from the short T2 species while the rest is from the longer T2 species (31). As in approximation, E_2 can to be replaced by a trenghted sum of two linex ponentials ($E_2 = 0.6 \times E_{21} + 0.4 \times E_{22}$); where $E_{21} \approx 1.5$ ins and $E_{22} \approx 20$ nm. T1 value for sodium also sho vs some variation (~25-40 ms). For simulations, a value of 35 ms was used (32).

The 60:40 ratio of short and long $\Gamma 2$ for sodium holds only in when motion of N⁺ is restricted in some fashion, either by a gel matrix of charged macromolecules. For human invivo studies, the above ratio was modified to 15:85 (chart:long T2) based on studies and e in perfused ex-vivo rat hearts (33). Extracellular volumed raction in the normal myocardium is

about 25%. The short T2 component in intracellular space is around 28% while it accounts for 11% of the entracellular codium. Sodium concentration in ECV is 144 mmol/L and 16 un tol/L in intracellular space. Combining these factors gives a 15% contribution from short T2 and 85% from the long T2 species in-vivo.

Off-resonance

Given the 'ow gyromagnetic ratio $(v_{Na}/v_H = 0.26)$ of sodium, it follows that sodium imaging is less susceptible to off-resonance effects resulting from field inhomogeneity or susceptibility. In addition, motion reluted spin dephasing would also be reduced by the same ractor (~ 4). In particular, chemical shift effects the over from shielding of protons in lipid are absent in sodium imaging. The above observations make sodium imaging over a longer cardiac phase possible. In addition, spiral imaging will show reduced motion artifacts even with longer acquisition windows compared to rectilinear regime. Assuming a variation of roughly ± 0.042 (Figure 3 in (34)) across the left ventricle for proton imaging at 3T, this corresponds to compared with traditional proton imaging.

Motion

The quiescent period of the cardiac cycle (corresponding to diastole) can vary from 60 ms to about 306 ms (35). Since mation related dephasing follows the same principles as offresonance, one would expect motion related dephasing follows the same principles as offimaging. Since resolution for sodium images is lower than proton images, partial volume effects will be present. However, as diac motion is greater during systole, so there exists a trade-off between motion related dephasing and increased ecceptance window. Despite the use of a gating window, mation related blurring will result in an underestimation of signal and overestimation of infarct zone. Finally, by changing the order of spiral arms in a predetermined to random result motion artifacts can be further reduced (36).

Methods

Excitation pulse

A modified 3D slab selective excitation pulse that allowed for a relatively should be used. The RF pulse was a truncated sine-gauss with one left side lober for shorter effective TE; pulse duration was 1.55 ms at a normal angle of 70° for sodium imaging the iterative solution (eq. [4]) for RF pulse train determination was introduced to determine the flip angles for echo train length in a realtime feation.

Sequence Determination

To resolve which of the two choices (A) or (Σ) provides better signal, $e \sin p(z) 1$ - D Eloch simulation was performed. Bloch simulations were performed using equations [2], [3] and [4] with TR increases in steps of z ms from 15 ms to z 0 ms. Since the coho in z changes with the flip angle (due to pulse stretching), echo time recorded for a particular inplangle was used in the Bloch simulations. Three sequence variations were considered: (A) Constant gradient-echo dephasing with constant flip angle from (B) Spoiled gradient with constant

For each TR (changed in steps of 5 n s) for sequence (A) and (B), the flip angle was varied (in steps of 5) to realize the maximum signal possible. Note that for the constant flip angle version of sequence B, the excitation angle does not necessarily correspond to the Ernst angle of $\alpha = \cos^{-1}(\exp(-TR/T1))$. This is because the minimum TE changes with the excitation angle. For sequence B with varying flip angle along the *etl*, the maximum flip angle (at $n = ct^{0}$) was varied in steps of 5° to determine the maximum signal for a given TR.

B1 Inhomogene ity

Our current work used a single transmit-receive surface poil which results in considerable PF field inbomogeneity that is disady integeous for clinical applications. As an alternative to correcting for it (which involves substantial acquisition time and post-processing), we modeled the B1 inhomogeneity resulting from a 50% drop from the prescribed angle for sequence: (A) and (B). The achieved maximum value of FoF was then compared to the flip angle for (A) and (B). This provided an indication of the SNR drop to be expected for a 3D acquisition for sinces away from the transmit/receive coil

Imaging Resolution

To determine imaging resolution as a function of relation and field inhomogeneity, the exact spiral trajectory (based on equation [1]) was simulated in Matlab®. The segmented trajectory — where a fraction of the total number of spiral chars (given by *etl*) is acquired per cardiac trigger — meant that relation, needed to be modified accordingly. Since the spiral arms were acquired in two shots (each shot duration = $2C^{\alpha}$ ms), the k-space locations resulting from such an acquisition, were modified to reflect the segmented nature of the acquisition. For example, magnetization for spiral arms 1,..., 18 Gor the case with 36 total arms) were calculated with initial magnetization $M_Z = 1$ for arm 1 and signal model for the 18 arms based on eqs. in [3]; M_z for arms 2-18 corresponded to recovered longitudinal magnetization from previous 1R. Spiral arms 19,..., 36 followed the some path on with initial M_z for arm 19 being 1 (Figure 5). Exact imaging parameter, were used to derive this PSF; values for TE, TR, Tacq and excitation angle were as recorded on the scanner. For example, for spiral sequence (B) with constant, inplane, when TR = 20 ms, spiral arms = 36 and flip angle = 35°, TE = 0.74 ms, Tacq = 15 ms and TFE factor (*etl*) - 18; when TR = 40 ms, spiral arms = 18 and flip = 40°, 1'E = 0.77 ms, Tacq = 35 ms, TFE factor = 9

Off-resonance effects were simulated by introducing the factor $(e^{-i\gamma\Delta^3}0^{-1})$ where $\Delta \mathcal{P}_0$ is the field inhomogeneity. The magnetization was consequently modified using $\Delta f = 13$ Uz (value derived earlier). The signal obtained in k-space was then reconstructed using the gridding algorithm described by Jackson et al (57). Someting density compensation is as performed

prior to gridding using a normalized density compensation factor calculated using $(k_x(t).g_x(t) + k_y(t) g_y(t))$. This was folle and by a 2D haverse Fourier transform. The reconstruction was implemented in Matlab®. The YWHMA (full width at half maximum) of the resulting PSF was used as an estimate for the final resolution, different from the nominal prescribed resolution

Inaging

Phar'.om studies—A.i imaging v as performed on a Philips 3T Achieva system equipped with a broadband amplifier with multinuclear c_{p} ability. A surface coil with an integrated transmit/receive rodium coil and a transmit/receive 'r' coil (Rapid Biomedical GmbH, Rimpar, Germany) was used. Coil dimensions were 27 cm (R/L) × 28 cm (F/H) for the sodium transmit coil while the receive coil halt dimensions of 18 ×18 cm. The Tx/Rx ¹H coil nau dimensions 23.5 × 23.5 cm. The maximum achie rable RF was 33 µT for the sodium coil and 12 to µ1 for the proton imaging coil. A tottle containing 4% agar 150 mM NaCl gel was imaged using a 5D protocol (16 slices) with slices along the coronal direction parallel to the coil. Imaging parameters were FOV = 30 cm, ECG galed acquisition (60 bpm) over 360 ms of cardiac cycle. The Leorresponding to sequences A1 A3 and B1-B3 (constant flip and optimized Tup); NSA = 16, prescribed resolution was 4 < 4 × 8 mm³, scan time 5:22. All comparison scans were performed in a lingle session since phantom positioning may otherwise result in variations in the measured SNR

Hum: n s'udies—Institutional review bound approval was obtained for human studies. Six volunteers were imaged in the prone position with cardinal reads attached to the back. A double oblique acan was used to establish the loft ventricular shout axis as well as the long axis. Nominal resolution and imaging window of the cardiac cycle was kept constant at $5 \times 5 \times 10 \text{ mm}^3$ and 360 ms, respectively. Other imaging parameters were: FOV $\approx 26 \text{ cm}$, $\alpha = 75^\circ$, TR/TE = 40^{-1} .02 ms, Tacq = 35 ms, spiral arrows = 16, fFE factor = 9, NSA = 22, number of overcontiguous clication = 10, scan time: 6-10 minutes (depending on heart rate). For comparison to reformatted (large axis) sodium in ages, long axis ¹H images were obtained using a single slice, multiple phase segmented gradient echo sequence with the following parameters: FOV = 40 cm, TR/TE = 4.4/1.2 r/s, $\alpha = 15^\circ$, par ial $c_y = 0.65$, res = $4 \times 4 \times 10 \text{ mm}^3$.

SNR measurements

In order to prevent any background filtering from offecting SNR measurements, reconstructed images were converted to complex data formation the scanner. The files were read off-line in a Matlab® program and SNR measurements were correct out by plucing ROIs in the object and the remote background. SNR was measured using standard formulation (S_{ROI}/σ_{ROI} where S_{PC_1} is the signal man ROI in tissue while σ_{ROI} refers to standard deviation of an ROI in the remote background).

Results

Phantum

Figure 1 shows the simulated and measured PSF with sequence A (SSFP-FID) for three different 'Rs (20, 30 and 40 ms) and constant lip angles 55°, 60° and 65°, respectively. The maximum in PSF was recorded for the given inp angles with the corresponding TR for the case when chort:long $T_{n}^{2} = 0.6:0.4$. Measured SNR for the three cases obtained from the phanto in study is shown to a square icon. The measured signal increased by 28.3% across the three TRs while the simulated signal increased oy 31.3%.

Figure ? plots the simulated and "Leasured PST for sequence B (SPGR) with constant flip angle as well as with the optimized flip angle other edescribed in the Theory section. Again three sample cases are considered for in ustrative purposes: (1) TR = 20 ms, flip = 35° (constant) flip = 15° (optimized train) (2) TR = 30° Liss, flip = 40° (constant), flip = 50° (optimized) and (2) TR = 40 ms, flip = 40° (const), flip = 50° (optimized). A square icon indicated with each PSF shows the measured SINK for each case. For both Figures 1 and 2, values were scaled to the simulated value for sequence 33 (optimized) in order to provide a casis for relative comparisons between all values (si null ted and measured). The difference in measured SNR between the constant and optimized rain for each TR was minimal. The mean difference in measured SNR between the theorem difference across the three sequences was 37%. The simulated afference across he three cases was 16.6%.

These results show that for both sequences (A) and (Σ), longer CRs result in higher SNR. In addition, sequence B (SPGR) perior ns slightly better than sequence (A) at each TR (Figures 1 and 2). Of note, the P_P angles corresponding to maximum signal strength are relatively higher with requence (A) indicating higher SAR deposition

Figure 3 shows simulated signal response for sequences (A) and (B) for flip angle variation from α_{max} to a power value of 0.50 μ_{max} . Figure 4 shows the measured SNR of slices obtained along the core nal direction (slices parallel to the contwith direction 6 being farthest from the coil). Both simulations and measurements indicate acquerce F (SPGR) with constant or optimized alip angle train provides better robustless to B1 inhomogeneity than sequence (A). In addition, the signal provided by either the constant or optimized train is very similar.

Relaxation and Off-resonance Effects

Since simulations and measurements showed that lowger TR imaging provides better SNR per unit time, the upper limit on TR was determined. Typically, relax tion and offeresonance effects will result in a bound on the acquisition window: (and therefore TR). Figure 5 shows the simulated k-space data for the spiral traincoury for sequence B1 vith constant fl p angle of 35°. Figures 6(A) shows the PSE for sequence B1 (SPG R), 6(B) shows the line provide through the PSF for the three sequences (B1), (B2) and (B3) with constant f ip angles The peak values for the PSF were 1.29, 1.55 and 1.72, respectively. This shows an improvement of about 37.5% (from TR = 20 ms to TR = 40 ms) which is close to the n easured improvement of 34.5%. FWHM for sequences B1, b2 and B3 was equal at 6.8 mm while

the nominal resolution mass imm. As described earlier, we consider a mean off-resonance of 13 Hz across the left ventricity. Simplations show that the peak of PSF deteriorates from 1.72 to 1.28 when TR = 40 n s while the nuck deteriorates from 1.29 to 1.23 for the shorter TR of 20 r.s. (FWHM stays the same at 0.8 mm.) This indicates that the relatively longer data acquisition of sequence B3 shall outperforms the shorter acquisition of sequence B1 despite increased in ain field inhomogeneity related signal loss. Any further increase in TR (or a further increase in field inhomogeneity) provides diminishing returns as one gets a better response from shorter Tr's sequences. For example, for TR = 50 ms, the maximum value of the PSF (normalized for short duration differences) decreases from 1.73 to 1.09 due to the assumed inhomogeneity. We considered a 1R of 40 ms as a reasonable compromise between increasing SNR versus off-resonance blurning and artifacts.

Figure 7 shows the line profile through an phantom reflecting the increased signal with increasing TP for SP β R sequence B1, B2 and β 3. No γ that no additional blurring is noticed (as at edge) with the increase.

In-vivo Imaging

In the in-vivo case with different ratio of short and long Γ^2 sodium, simulations show a similar trend of increasing signal with increasing TR. The optimal TR based on offresonance consideration is again 40 ms. However, the $f^{12}_{\mu\nu}$ angle at which maximum signal is observed for the SPGR sequence with constant excitation angle was 75°. Using an optimal flip angle train gave maximum signal when the final angle way 80°. Maximum of PSF obtained by simulating along the spiral acquisition trajectory provided a slight edge for the constant flip angle case (~4% higher). When off resonance was considered, PSF_{max} dropped by 25% for constant excitation SPGi' sequence

SSFP-FID schuence provided a slightly higher PS r_{max} at an optimal excitation angle of 90° (~2.6%) when compared with constant excitation angle SPGR. However, SSFP-FID suffers from greater signal reduction due to B₀ and B₁ inhomogeneity. As a result, sequence B3 (SPGR) with flip angle of .'5° was used for in-vivo invasing. FWHI 1 was the same for all sequences considered,

Imaging

Figure 8 shows the first 8 images (out of 16) obtained using the sodium phantom what sequence B3 (SPGR). The decrease in SNLK with increasing distance from the call is apparent. The measured SNR for the first 8 slices was 43.1 while is it was 33.5 across all 16 slices. Figure 9A shows sample short axis sodium in ages obtained from a volunte in Figure 9B compares a reformatted long axis free of the sodium images with a corresponding longaxis ¹H image obtained at approximately the same cardiac phase. Bot himages are copped and scaled to the same dimensions.

The measured SNR in the septum over all slices where the septum was dc_r^{-1} and for the six volunteers was 17 ± 1.7 .

Discussion

In vive sodium MRI requires extender scan times to realize sufficient SNR. In particular, sod.um maging of the heart requires efficient use of scanning time primarily to counter artifacts 1 om patient motion (cardiac and roop ratory motion, patient movement and patientcoil disple, ement) which spically increase with increasing scan time. Hence traversing the k-space in a fast, efficient manner is in portant. Since sodium T2 time is relatively short, a s an technique that is robust to mot on and provid, s a short echo time is paramount. Stack of spirals imaging fulfills all the above criteria. Since the T1 of sodium is short ($\sim 25-40$ ms), 3D comming provides near the concal VN cuvantage over corresponding N-slice 2D imaging A fururable convergence of factors directly resulting from the gyromagnetic ratio (γ) of sodium being about one-fourt¹, of γ for provides allows for extended data acquisition (of the order of T1 value) conducive to sp. ral i naging. Given the myriad number of combinations of poss ble MR parameters, E loch equation simulations help to determine maxim im medicted SNR in the setting of signal loss from relaxation effects, off-resonance and motion. Operating near the maximum P1 output of the sodium coil ensures lowest prosible .cho time. Counter-intuitively constructoritation angle with a spoiled gradientche spiral performed better than an optimized flip angle train that aimed to keep magnetization constant from one repet tion time to the next. On closer inspection, one can survise and steady-state magnetization is cohieved fairly apidly for sodium since $T1 \sim TR$. As a result, a larger final excitation angle for the optimal curitation train results in marginally longer echo time and provides the constant flip and le train sequence a slight edge. A similar advantage is seen with relation to RF home condity; larger flip angles employed vith sequence A resulted in more rapid fail off in excitation over a range of flip angles.

Relaxation and off-resonance can be studied by draiving the chart PJF. Although the absolute values of the PSF will change as a function of resolution, the relative PSF values depend only of relaxation properties, fiel inhomogeneity, excitation angle, echo time, repetition time and data actualities window. For example, when in June resolution was 5×5 mm², for TR = 40 ms, the n salmura PSF ranged from 1.59 to 1.19 with Δ^{c} = 13 Hz. For TR = 20 ms, the PSF maximum ranged from 1 22 to 1.16, thus naintaining, the trend. The FWHM was 7.9 mm for all I'Rs considere 1. While the F.V'Hist does not enange with offresonance, PSF side lo'ses show increased amplitude and ripple streets. Note that the maximum PSF actually decreased from 1.72 to 1.59 when the special resolution changed from 4×4 mm² to 5×5 m. n². This may be counterin tuitive, but the signal is remercined by the total volume under the rSF, approximated as $\Gamma_{S,F_{max}} \times (\pi < F'_{MM} HM^{2/2})$; this gives a 25% higher value for the 5×5 mm² case versus 4×1 mm². Slice thickness mas not considered in the optimization as it has probleming or sequence parameters except for the total duration of the scan. Since each slice encluing is dequired in two shots, the number of slices will dictate the total scan time while 3D stab dimension (clice direction) affects the SNV. Ir this study, the number of spiral interleaves for a fixed TR was leld constant. Ere possible to trade the number of interleaves with signal werages. For example, when TR = 40 ms, number of interleaves was fixed at 18 (etl = 9). If 1.5^{A} is 10, number of interleaves could be increased to 36 (etl = 9) and NSA dropped to 8 in keep total scan time constant. Our simulations and phantom as well as in-vivo measurements showed minor charges resulting from such

Gai et al.

variations in combinations of interfeaves and NSA. For example, three combinations of interfeaves and 1 is As were used (interfeaves = 18, 9, 36; corresponding NSAs = 16, 32, 8). An xim in difference in SN1' was 7% with the combination used in our experiments above providing the highest SNR. This is because in non-Cartesian sampling schemes such as radial or spiral imaging, increasing the minimer of spokes or interleaves acts as averaging cline each, poke or aim is merely a rotated version of any other spoke or arm.

The contribution to total so that signal from the first relaxing sodium was calculated to be 15% based on studies in the reperfused rate neart. Nr studies on the ratio of fast to slow T2 contributions na re been done in humans since toxic shift reagants are required to isolate the short and long 12 contributions There is evidence that interspecies variation in the ratio does exist (38). A different ratio of (25:75) provided the same optimal solution although simulations choused a drop in signal of 11.5% over the (1.5:85) case as expected. ECV in infarcted mycocritium can be much higher $\sqrt{-0.5}$ (39)). Accordingly, we studied the effect of the corresponding ratio (11:89) using simulations. Optimal solution (TR = 40ms, $\alpha = 75^{\circ}$) stayed the same while the signal was 2.85 times night due to the much higher total sodium concentration as well as slightly increased concentration of long sodium T2 species. In ddition, results obtained from phantom and volunteer studies were consistent with observations from simulations providing indirect support for the assumptions used in the sin ulations. In the six volunteers, the SNP for sequences 51, B2 and B3 was derived from ROL placed on the ventricular septum. The SNP, for B2 v. 33% higher than for B1 and 47% light for B3 compared to 31. Simulations chowed ancreases of 20% (B2 vs B1) and 34% (EC vs B¹). Since R^F innomogeneity is a significant f_{2} to in the measured SNR, it is possible that the Cip angle at which SNR is maximum can be unfferent from the one derived through si nult tions. However, the difference is minut for a fixed 'R and small changes in the excitation alighe For example, in phantom experiments, a flip angle of 55° (instead of 40°) resulted in a small arop in SNR (3%).

The relatively long ecno time that was used will result in some loss of the sodium signal (about 25% of the was' signal for the phantom and 12% the nervivo i maging). The echo time was determined by two factors: (a) 'ardware limitation and (b) en couing scheme. Since the nutation angle is given by $\alpha = \frac{1}{2}B1(t)dt$, the B1(t) field for sodium see ds to be about four times that for proton imaging to achieve the same nutation angle. However, the peak B1 delivered by the ¹H coin is 13.5 μ T while that delivered by the Ma coil is 53 μ T. This limitation means that the RF pulce is about 1.6 times longer for Na imaging than the corresponding pulse for proton imaging. Using a pon-selective excitation purce to and in aliasing artifacts and minor reduction in scan time. A nother factor that increased the scho time by ~0.3 ms was the need to perform κ_7 encoding with a stack of spiral. A k-space trajectory similar to the cushball radial imaging trajectory but with spiral arms for officient coverage would result in a short: echo time. A modified radial trajectory with longer data acquisition has been proposed recerily (7) in addition, earlier works have looked rcoptimization based on T2 and fiel inhomogeneity effects for density adapted radial trajectory (40,41). However, as noted earlier, the stack trajectory may be bet er suited for cardiac geometry in that it covers a cylindrical space allowing for thicker slices along the long axis of the heart.

Gai et al.

RF field inhomogeneity exacerbated by the use of a single channel surface coil resulted in a large variation in the measured Give. For example, the SNR varied from 24.2 to 11.1 in the vertricular septum over all slices for a study subject. Previous studies have shown that the human events is capable of discerning objects from the background with 100% certainty when the SAR > 5 (the Rose criterion (42)). The signal in the septum was well above this threshold for all volumeers. However, signal in the posterior wall away from the coil can fall below the threshold for sinces. Improve nents in coil design and correction techniques should overcome this deficiency. Total sodulum concentration can only be determined when some technique for compensation of RF information and be employed.

One earlier work studied the advantage of retrospective (as opposed to prospective) gating for improving SNR (16). In our work, the window for the echo train to be played out was fixed at 260 mm. One would expect this time window to change with the heart rate. The number of spiral arms can be varied to change twis window. For example, for TR = 40 ms and heart rate of 70 bpm, it would be possible to drop the number of arms by 1 (to 8) making the veho train time 320 ms. On the other hand, it could be increased to 400 ms with a lower heart rate. It is not clear whether using continuous constriggered acquisition is beneficial. Our observations over a limited data set were inconclusive. In some subjects, image SNR with continuous scanning led to improved definition of the distal parts of myocardium. Ho vevel, in other volunteers, non-triggered images exhibited greatly increased blurring and partial volume effects, negating any beneficial effects of improved SNR.

Earlier works on 2D sodium imaging of the heart have exhibited shortcomings. While 3D imaging of the heart was accomplished in 54 mins in (12), the cork of (14) showed just one cardiac in age from the 3D data core. TPI of the heart is more efficient (5); however, only a single slice with a hot color map or creation on proton images makes it difficult to ascertain image quality (Figure 2 in (5)). A measure of the SixR was about of provided.

Conclusions

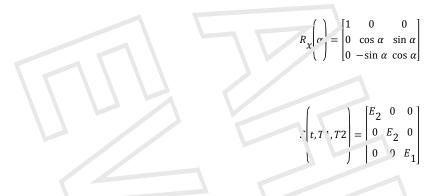
Simulations for optimil ation of parameters of a 3D stack of uplicals requerce allows for the entire human heart to be imaged in about 6-10 minutes. To one knowledge, this work presents the first multiple cardiac sodium images from a full 3D soft and the consequent reformatted images.

Acknowledgments

The authors would like to acknowledge Dr. Yuxi Pang, Dr. Christ an Stehning on LDr. Michael Schar of Anilips Medical Systems and Marco Irkens of Rapid Biomodical for inition help with the order. This work was supported by the intramural research program of the Clinical Center at Naci.

Appendix

$$R_{Z}\left(\gamma\right) = \begin{bmatrix} \cos\varphi & \sin\varphi & 0\\ -\sin\varphi & \cos\varphi & 0\\ 1 & 0 & 0 & 1 \end{bmatrix}$$



References

- 1. Furtish 1D, Fleno DS, Fitzgerald SW, Judd I M. Theoret call asis for sodium and potassium MRI of the human base i at 15 T. Magn Reson Med. 1997; 38(4): 55-661. [PubMed: 9324333]
- 2. Polin eni ^P1. Extracellular space and ionic distribution in rat ventricle. Am J Physiol. 1974; 227(3): 676–653. [P¹5Med: 4413398]
- 3. Cawerkrak R. Sodium MRI. Methods Me' Biol. 2011; 711, 175–201. [PubMed: 21279602]
- Koc' atte CE, Kir, KJ, Hill nbrand HB, Cher EL, Lima IA. Microvascular integrity and the time course of inyocardial sodium accumula ion after acute infarction. Circ Res. 2000; 87(8):648–655. ["ubMed: 11029399]
- 5. Cuwe kerk R, Bottomley PA, Solaiyappan M, Specher AF, Tothaselli GF, Wu KC, Weiss RG. Thisue rodium concentration in myocardial infarction in human a quantitative 23Na MR imaging study. R rdiology. 2008; 24%(1):88–96. [Publ red: 1856/11]
- Inglese M., Madellin, G., Oesinghann N., Babbull, Wu W., Stoecker P. Herbert J, Johnson G. Brain tissue sodirin conceptuation in multiple sclerosis: a sodium imaging study at 3 tesla. Brain. 2010; 133(Pt 3):847-557. [PubMed: 20110245]
- 7. Konstan lin S Nagel AM, Heller PM, Schad LR. We Jumensional radial acquisition technique with density a laptic n in sedium MRL ling Reson Med. 2011: 65 (+):1090-1096. [PubMed: 21413073]
- 8. Haneder S, Konstandin S, Morelli JN, Nagel AM, Z eitner FG. Senad Lk. Schoenberg SO, Michaely HJ. Quantitative and qualitative (23)Na Mi Luaging of the num in kidneys at 3 T: before and after a water load. Publicity 2011; 2t 9(3):857–865. [Publicited: 2177 1954]
- 9. Nielles-Vallespin S. Weber MA, Doil, M. Pongers A, Sheier P. Combs SF. Wohrle J, Lehmann-Horn F, Essig M, Schall LR 3D adial relojection technique with ultrashort ec. 2 times for sodium MRI: clinical applications in human orain and skeletal muscle. Magn Peson. Med. 2007; 57(1):74– 81. [PubMed: 17191248]
- Boada FE, Shen GY, Charg SY, Thulborn KR. "pectrally weighted wisted projection imaging: reducing T2 signal http://uation effects in fas three-dimensional sodium. Imaging. Lagn Peson Med. 1997; 38(6):1022–1028. [PubMad: 9402205]
- 11. Ouwerkerk R, Weiss RG, Bettomley PA Areas tring human cardie a tissue software contentrations using surface coils, adiabatic evolution, and twisted projection i naging with minimal 72 torses. J Magn Reson Imaging, 2005; 21(5):546–555. [Publical: 1583491.]
- Pabst T, Sandstede J, Beer M, Kenn W. C. user A, vor. Kienlin M, Neuoauer S. Van i D. Optimization of ECG-triggered 25 (23)Na MCu of the human heart. Magur Reson Med. 2001; 45(1):164–166. [PubMed: 1:146499]
- Sandstede JJ, Hillenbrand H, Beer M, Paost T, Butter F, Machann W, Barler W, Halln D, Neubauer S. Time course of 23Na signal intersity after myocardial infarction in httmatis. N'aga R son Med. 2004; 52(3):545–551. [PubMed: 15334373]
- Jerecic R, Bock M, Nielles-Valles bin S, Wacker C, Bauer W. Schad LR. ECG-ga ed 25Na-MCa of the human heart using a 3D-radial projection technique with ultra-short echo times MAGMA 2004; 16(6):297–302. [PubMed: 15160295]

- 15. Qian Y, Zhao T. Zheng T, Weiner J, Boach FE. High-resolution sodium imaging of human brain at 7 Γ. Magn Re on Med. 2012: 68(1):227–2: 3. [PubMed: 22144258]
- 16 Koi standin, S.; Schao LR. 2D radial scalum heart MRI: Prospective vs retrospective ECG-gating using golden angle inclements; Proceedings of the 20th Annual Meeting of ISMRM; Melbourne, a ustralia. 2012; p. 1696
- 17. Jerecie, R.; Bock, M., Zabe', H-J.; Scha¹, LR. T. me resolved sodium imaging of the human heart at 1.5⁻, Proceeding: of ane 8th Annual Meeting of ISMRM; Denver, Colorado. 2000; p. 1651
- A'.n CB Kim JH, Che Zin. High-speed spiral-scan echo planar NMR imaging-I. IEEE Trans Med Imaging. 1986; 5(1):2-7. [PauMed. 182 (3976]]
- ¹⁹. ¹ eyer CH, Hu BS, Nishimura DG, Maco Cin A. Fast spiral coronary artery imaging. Magn Reson Med. 1997. 28(2):202–213. [PubM.u: 1461122]
- 20. King KF, Foo 'K, Crawfo a CR. Optimized gradie a we veforms for spiral scanning. Magn Reson Med. 1995; 34(2):156–160. [PaoMed: 74750/3]
- 21. Cline HE, Zong X, Gai N. Design of a logarith unc k-space spiral trajectory. Magn Reson Med. 2001; ACC).1126-1135. [Publ fed: 117+6579]
- 22. Vlaardingerbroek, N'T.; den Boer, JA. Magnotic 1'esona. 1 maging: Theory and Practice. Spinger Berlin 1997. p. 1169-1180.
- 23. Born at P, Schomberg H, Aldefeld B, Groen J. Improvements in spiral MR imaging. MAGMA. 999; 9(1-2):29–41. [PubMed: 10555171]
- 2.4. van der Meulen P, Groen IP, Tinus AM, Brutlank G. Fast Field Echo imaging: an overview and contrast calculations Magn Reson Imaging, 1988; 6(1):355–368. [PubMed: 3054380]
- 25 Luxton RP Euelman RR, Rosen BR, Vismer CL, Brady TJ. Contrast in rapid MR imaging: T1and T2-weighted imaging. J Comput Assist Tomog. 1987; 12(1):7–16. [PubMed: 3805431]
- 26. Ernst RR, Anderson WA. Application of Fourier transform spectroscopy to Magnetic Resonance. R v Sci Instrum. 1966; 37(1):1).
- 27. Freemar R, Hill The Phase and intensity and houses in Fourier transform NMR. J Magn Reson. 1971; 4:36 5-383.
- 28. Stehling MK Improved signal in "snapshot" FI AGH by variable fly angles. Magn Reson Imagin 3, 1992; 10(1):165-167. [Put Med: 1545(77]
- 29. Kemp-Larper R. Styles P, Wimpons S. Measurement of 222 a transvirse relaxation in vivo. The flip angle independent experiment. J Magn Reson Cories B. 1005, 109:2-3–228.
- Constantinides CD, Gillen JS, Boada FE, Pomper MC, Bottomley P.A. Hi man skeletal muscle: sodium MR imaging and quanuncation-p itential applications in exercise and disease. Radiology. 2000; 216(2):559–568. [PubMed: 109245) 6]
- 31. Berendsen HJ, Edzes 'HT. The observation and general interpretation of sodium magnetic resonance in biologica' material. Ann N Y Acad Sci. 1973 (204:459-485, [Put Med: 4513164])
- 32. Pabst T, Sandstede J, Peer M Kenn W, Neusau er S, Hahn D. Lvalu, tion Sr sod um T1 relaxation times in human he at. J Magn Reson Imaging. 2003; 17(6): 726–727. [PubMod: 12766903]
- 33. Van Emous JG, Van Fonteld CJ. Changes of intravellular sod um T² cetaxation times during ischemia and reperfusion in isolated nat hearts. Magn Reson Med. 1998; 70(5):679-565. [PubMed: 9797149]
- 34. Sung K, Lee HL, Hu Hi I, Nayuk KS. Prediction of myocardial signal during CIN 3 balancea SFP imaging. MAGMA. 2010; 23(2):85–91. [PubMod. 20. 29086]
- Johnson KR, Patel SJ, Whigham A, Holdin A, Pettigrew RI, Oshinski JN. Thrue-din ensional, time-resolved motion of the colonary arterius. J Cardiovasc Magn Reson. 2004; 6(2):563–673. [PubMed: 15347131]
- 36. Pipe JG, Ahunbay E, Menon P. Effect, of interland order for spiral MRI of dyr at the processes. Magn Reson Med. 1999; 41(2):417-422 [rubMed: 10080253]
- 37. Jackson JI, Meyer CH, Nishimura DG Macovski A. Sel ctio of a convolution function for Fourier inversion using gridding computerised tomography application]. IEEE Trans Med Imaging. 1991; 10(3):473–478. [FibMed: 18222000]
- Foy BD, Burstein D. Interstitial sodium nuclear mag. etic resolution relaxation times in perfused hearts. Biophys J. 1990; 58(1):127–134. [PubMed: 2205027]

- 39. Arheden H, Saeed M, ^{L1} C, Gao D V, Bremerich J, Wyttenbach R, Dae MW, Wendland MF. M easurement of the distribution volume of gadopentetate dimeglumine at echo-planar MR imaging to quantity n yocardial *i*-atarctive: comparison with 99mTc-DTPA autoradiography in rats. Rad. plogy. 1999; 211(.):69? /08. [2 ubMed: 10352594]
- 40. Nagel AM, Laun FB, W ber M^{*}, Matthies C, Semmler W, Schad LR. Sodium MRI using a density-adapted 3D^{*} adial *e* quisition technique. Magn Reson Med. 2009; 62(6):1565–1573. [PubM.1: 1985991.]
- 41. Ke istand n S, Nagel AM. reformance of sampling density-weighted and postfiltered densityadapted projection reconstruction is soo um magnetic resonance imaging. Magn Reson Med. 2°,13; 69(2):495–502. [rubMed: 224737(8]
- 12. Rose, A. Vision: human and electronic. Plenum: New York: 1973.



Figure 1

The vignt l resulting from sequence A (SSFP-FID) with three different TR times: (A1): TR = .'0 ms flip = 55°; (A.') TP = 30 ms flip = 60° and (A3) TR = 40 ms, flip = 65°. The square boxes near the corresponding peaks match the measured SNR scaled to the value obtained from the simulated signal for signature B3(opt) (see Figure 2).



Figure 2.

A: The signal resulting from sequence R (SPGR) with an optimized flip angle scheme. Simpluted signal from different TR time: are thown: (B1): TR = 20 ms, flip = 45° (max); (52) TR = 30 ms, flip = 50° (max): and (B3) TP. - 40 ms, flip = 50° (max). The square poxes near the corresponding peaks mark measured is NR from the phantom scaled to the value obtained from the simplude signal for sequence R3(opt).

B: The signal resulting from sequence B (SPC R) with a constant flip angle scheme. Summated signal from different TP, times are shown: (B1): TR = 20 ms, flip = 35° ; (B2) TR 30 n.s., flip = 40° . and (B3) TR = 40 ms, f. ip = 40° . The square boxes near the concesporting r caks mark measured SNR from the phantom normalized to the value obtained from the simulated signal for sequence B3.

Figure 3

Similated change in signal as a nunction of a change in the excitation angle as would be expected one to B1 in homogeneity. A polynom all of order three was fit to get a smooth variation. $\alpha_{1,vax}$ is the optimed inplanable as determined through simulations. TR = 40 ms for both secretores. The RF spoiled gradient echo sequence shows better B1 robustness compared with sequence A (SSFP-F.D).

Figure 4

Measured B1 inhomogeneity characteristics for the three sequences for TR = 40 ms. Measurements were taken in coronal clices parallel to the sodium coil. From the above, it's apparent that sequence B3 (constant excitation or optimized train) provides better signal in the presence of RF inhomogeneity.

Fig. re 5

Similated k-space data for the exact spiral trajectory used for data acquisition. TR = 20 ms, TE = 0.74 ms, spiral trajectory and leng h = 18. Two shot acquisition and T2 relaxation effects can be easily perceived as the signal evolves from the center of k-space.



Figure F.

(A) LSF resulting from tata accelle d with sequence B1: TR = 20ms, flip angle = 35°, 36 spiral arms, echo train length = 18. Peak values of the PSF was 1.29. FWHM was 6.8 mm. (5) Line profile through PSF (at y = .50 mm) resulting from data acquired with the three SPGR sequences B1: TR = 20 ms, flip angle = 35°, 50 spiral arms, echo train length (*etl*) = 10, B2: TR = 30 ms, flip angle = 40°, 24 spiral arms, etl = 12 and B3: TR = 40 ms, flip angle = 40°, 18 spiral arms, etl = 9. Peak values for PSF were 1.72, 1.59 and 1.29, respectively. If wHM was 6.8 mm for all three cases. Only the central 100 mm of FOV (= 300 mm) is shown.



Figure 7

Line profile through impge 5 (c, 16 slices) for a NaCl/agar phantom obtained from three SPGR cuprences B1, B2 and B3 with a constant flip angle train. Increased TR from B1 (TR=20ms) to B3 (TR = 40ms) does not result in increased blurring from T2 effects. Line profile was obtained by taking the mean of 20 line profiles (to reduce noise variation) around the center of the image.

Fig. re 8

Eight contiguous slices (jut of 16 slices) of the sodium phantom obtained using a 3D spiral requerce with optimized sequence values: TR/ E = 40/0.77 ms, 18 spiral arms with etl = 9, res: $4 \times 4 \times 8$ mm³, NCA = 15. Total scala time: 5 min 22 s. All images with constant window/level = 1200/600.



Figure °.

(A): Six (c. 18) slices obtained along the short axis from a human volunteer (57 kg female) using the optimized 3D spiral sequence. True thomisal resolution was $5 \times 5 \times 10 \text{ mm}^3$ (reconstructed: $5 \times 5 \times 5 \text{ mm}^3$). Total imaging time: 8:50. The images have been thresholded to reduce background noise

(D): Reformatted view (long LAIS) of the 16 slices (sod.um imaging) shows the LV and RV. (Location of short axis images of figure 9(A) are shown as dashed lines on the long axis image.) The entire volume (of 50 Lan from apex to b se) vas acquired in 8 min 50s. On Light i, une 1P long LAIS image of a single slice (long axis view) acquired with the same volume or results with the same volume results shows dimension in cm for both images.